

# PrimEx $\eta$ electromagnetic calorimeter, prototype for experiments at Jefferson Lab <sup>☆</sup>

A.Asaturyan<sup>a</sup>, F.Barbosa<sup>c</sup>, V.Berdnikov<sup>b</sup>, J.Crafts<sup>g</sup>, H.Egiyan<sup>c</sup>, L.Gan<sup>f</sup>, A.Gasparian<sup>g</sup>, T.Horn<sup>b</sup>, H.Mkrtchyan<sup>a</sup>, Z.Papandreou<sup>e</sup>, V. Popov<sup>c</sup>, S.Taylor<sup>c</sup>, N.Sandoval<sup>c</sup>, A.Somov<sup>c,\*</sup>, S.Somov<sup>d</sup>, A. Smith<sup>h</sup>, C. Stanislav<sup>c</sup>, H. Voskanyan<sup>a</sup>, T. Whitlatch<sup>c</sup>, S. Worthington<sup>c</sup>

<sup>a</sup>A. I. Alikhanian National Science Laboratory (Yerevan Physics Institute), 0036 Yerevan, Armenia

<sup>b</sup>Catholic University of America, Washington, DC 20064, USA

<sup>c</sup>Thomas Jefferson National Accelerator Facility, Newport News, VA 23606, USA

<sup>d</sup>National Research Nuclear University MEPhI, Moscow, Russia

<sup>e</sup>University of Regina, Regina, Saskatchewan, Canada S4S 0A2

<sup>f</sup>University of North Carolina at Wilmington, Wilmington, NC 28403, USA

<sup>g</sup>North Carolina A&T State University, Greensboro, NC 27411, USA

<sup>h</sup>Duke University, Durham, North Carolina 27708, USA

## Abstract

The article presents the design and performance of the electromagnetic calorimeter constructed for the PrimEx  $\eta$  experiment at Jefferson lab. The calorimeter was integrated to the DAQ and trigger system of the GlueX detector and used in the experiment to reconstruct Compton events. The calorimeter consists of 140 lead tungstate (PbWO<sub>4</sub>) scintillating crystals produced by Shanghai Institute of Ceramics. The calorimeter is a large-scale prototype of the two detectors, which are being currently constructed in the laboratory using similar type of crystals: the Neutral Particle Spectrometer (NPS) and the lead tungstate insert of the Forward Calorimeter (FCAL) of the GlueX detector. We will give an overview of the status of these projects.

**Keywords:** Electromagnetic calorimeters, lead-tungstate crystals

## 1. Introduction

The physics goal of the PrimEx  $\eta$  experiment in Hall D at Jefferson Lab is to perform a precision measurement of the  $\eta \rightarrow \gamma\gamma$  decay width. The measurement will provide an important test of QCD symmetries and is essential for the determination of fundamental properties such as the ratios of the light quark masses and the  $\eta$ - $\eta'$  mixing angle. The decay width will be extracted from the measurement of the production cross section of  $\eta$  mesons in the Coulomb field of a nucleus by photons, which is known as the Primakoff effect.  $\eta$  mesons are produced in a liquid helium target by a tagged photon beam with the energy between 10.5 – 11.7 GeV and is reconstructed by detecting two decay photons in the forward calorimeter (FCAL) of the GlueX detector. The cross section will be normalized using the Compton process, which will also be used to monitor the luminosity and control the detector stability during the run. In order to reconstruct the Compton scattering photon and recoiled electron at small angles we built a small (24 cm x 24 cm) calorimeter referred to as the Compton calorimeter (CCAL) and positioned it 6 m downstream the beam of the GlueX forward calorimeter. The CCAL consists of an array of 12 x 12 lead tungstate (PbWO<sub>4</sub>) scintillating crystals, which have been recently produced by Shanghai Institute of Ceramics (SICCAS).

The PrimEx  $\eta$  experiment started collecting data in Spring of 2019 using a He target and has acquired about 30% of the required statistics.

The Compton calorimeter is a prototype of the large-scale (PbWO<sub>4</sub>) calorimeter, which will be used to upgrade the inner part of the GlueX FCAL, which is currently instrumented with lead glass modules. This upgrade is required by the future physics program of Hall D, specifically the new experiment to study rare decays of  $\eta$  mesons[]. Integrated to the GlueX DAQ the CCAL performance was tested using the nominal GlueX running conditions. This allowed up to perform measurements of realistic rates and PMT anode currents in the FCAL insert region. The measurements will be used to tune the design of the front end electronics.

The Compton calorimeter was constructed in cooperation with the Jefferson Lab group working on the Neutral Particle Spectrometer (NPS), currently constructed in the experimental Hall C at Jefferson Lab. The NPS will use lead tungstate crystals with the same size provided by two vendors SICCAS and CRYTUR from Czech republic. The spectrometer will be equipped with the same photodetectors, Hamamatsu PMT4125, and read out electronics.

In Section 2, we will present the design and performance of the Compton calorimeter during PrimEx  $\eta$  run. Status of the FCAL upgrade project will be described in Section 3. Specifications of the Neutral Particle Spectrometer will be discussed in Section 4.

<sup>☆</sup>Notice: Authored by Jefferson Science Associates, LLC under U.S. DOE Contract No. DE-AC05-06OR23177. The U.S. Government retains a non-exclusive, paid-up, irrevocable, world-wide license to publish or reproduce this manuscript for U.S. Government purposes.

\*Corresponding author. Tel.: +1 757 269 5553; fax: +1 757 269 6331.

Email address: somov@jlab.org (A.Somov)

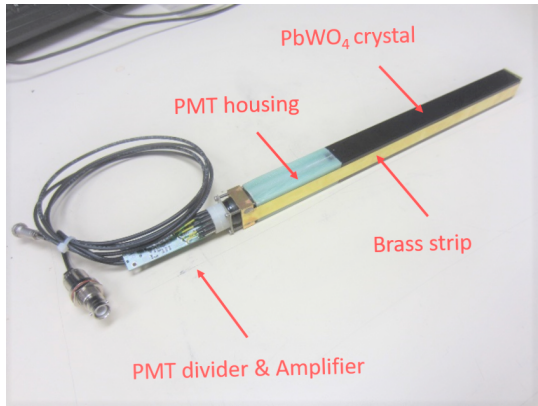


Figure 1: Calorimeter module.

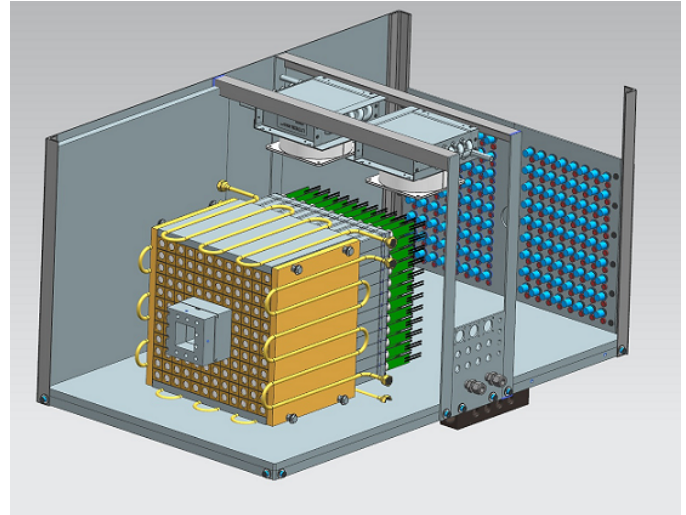


Figure 2: Schematic layout of the Compton calorimeter.

## 2. Compton calorimeter of the PrimEx $\eta$ experiment

The main purpose of the Compton calorimeter is to provide a fast trigger and perform reconstruction of Compton events. The CCAL is positioned behind the GlueX forward calorimeter, about 12 m from the target, and covers the angular range between  $0.18^\circ$  and  $0.33^\circ$ . An electrons and photon originating from Compton events are produced at small angles and are predominantly detected by the CCAL and FCAL, respectively. Schematic view of the GlueX detector and the Compton calorimeter is illustrated in Fig. 1

### 2.1. Module design

Design of the  $\text{PbWO}_4$  module is based on the HyCal calorimeter, which was used in several experiments in Hall B []. Assembled calorimeter module is presented in Fig. 1. The lead tungstate crystal is wrapped with a  $60 \mu\text{m}$  polymer Enhanced Specular Reflector film (ESR) manufactured by  $3\text{M}^{\text{TM}}$ , which allows to achieve 98.5% reflectivity across the visible spectrum. In order to improve optical isolation of each module from its neighbors, each crystal was wrapped with a  $25 \mu\text{m}$  thick Tedlar. The crystal is attached to the PMT housing which is made from G10 fiberglass. Two flanges are positioned at the crystal and housing ends and are connected together using  $25 \mu\text{m}$  brass straps, which are brazed to the sides of the flanges. Four set screws are applied to the PMT housing flange to generate the tension in the straps and hold the assembly together. Light from the crystal is detected using a ten-stage Hamamatsu PMT 4125, which is inserted to the housing and is coupled to the crystal using an optical grease. The PMT diameter is 19 mm. The PMT is pushed towards the crystal by using a G10 retaining plate attached to the back of the PMT and four tension screws applied to the PMT flange. The PMT is instrumented with the high voltage divider and amplifier positioned on the same printed circuit board, which is attached to the PMT socket.

### 2.2. Calorimeter Design

The calorimeter design is shown in Fig. 2. An array of  $12 \times 12$  calorimeter modules with a  $2 \times 2$  hole in the middle for the

photon beam are positioned inside the light tight box. A Tungsten absorber is placed in front of the innermost layer closest to the beamline. The light yield from  $\text{PbWO}_4$  crystals depends on the temperature with the typical temperature coefficient of  $2\%/^\circ\text{C}$  at room temperature. Maintaining constant temperature is essential for the calorimeter operation. Calorimeter modules are surrounded by four copper plates with built in pipes to circulate the cool liquid and provide temperature stabilization. An insulator was used around the detector box. The temperature was monitored and recorded during the experiment by four thermocouples attached to different points of the module assembly. During the experiment temperature was maintained at  $17 \pm 0.2^\circ\text{C}$ . In order to prevent condensation, the nitrogen purge was applied. Two fans with the water-based cooling system were installed on the top of the crystal assembly to improve nitrogen circulation and heat dissipation from PMT dividers. The detector was position on the movable platform, which provides motion in the vertical and horizontal directions perpendicular to the beam. During detector calibration, each module was moved to the beam.

### 2.3. Electronics

The PMT of each calorimeter module is equipped with the active base prototype [1], which was designed for the lead tungstate calorimeter of the Neutral-Particle Spectrometer (NPS) in the Jefferson Lab experimental Hall C. The base combines a voltage divider and an amplifier powered by the current flowing through the divider. The active base allows to operate the PMT at smaller voltage and consequently at lower anode current and improves the detector rate capability. Operation of the PMT at smaller anode current is also important for the extension of the photomultiplier tube life. The active base circuit contains 5 bipolar transistors, three in the amplifier circuit and two on the last two dynodes of the voltage divider, which provide gain stabilization at high rate. Active bases from the NPS detector have a relatively large amplification of about a factor

of 24 due to the large PMT count rate predicted by Monte Carlo simulation. During PrimEx run, the CCAL was operated at the HV of about 680 V and the divider current of 260  $\mu$ A.

Amplified PMT signals are digitized using a twelve-bit multi-channel flash ADCs operated at a sampling rate of 250 MHz [4]. The flash ADCs are positioned in the VXS crate. An example of the flash ADC signal pulse obtained from a calorimeter module is shown in Fig. 4. The calorimeter was integrated to the trigger system. The trigger is based on the energy deposition in the Compton and Forward calorimeters.

#### 2.4. Light Monitoring System

To monitor performance of each calorimeter channel, we designed and installed an LED based light monitoring system (LMS). The LMS optics includes a blue LED, spherical lens to correct the conical dispersion of the LED, and a diffusion grating to homogenize the light. Light was incident on a bundle of plastic optical fibers (Edmund Optics) with the core diameter of 250  $\mu$ m. Each fiber distributes light to the individual calorimeter module. On the crystal end, the fiber is attached to the module using a small acrylic cap glued to the crystal with a hole drilled through each cap to hold the fiber inside.

To monitor stability of the LED, we use two reference Hamamatsu 4125 PMTs. Each PMT has a single fiber from the LED attached to their front face as well as one of the YAP:Ce scintillator sources. The PMTs were read out using flash ADC. HV on each PMT was adjusted in such a way to make signals from both the LED and the  $\alpha$  source fit to the flash ADC range, as shown in Fig. 1. Each LED was driven by a CAEN 1495 module.

The LMS system was integrated to the GlueX trigger system and allowed to produce a special trigger type during data taking. The LMS system was extensively used during the detector commissioning and was running in parallel to the data production run injecting light to the detector with a typical frequency of 100 Hz. Stability of the LED system for the entire PrimEx run was measured to be better than 0.5 %. The ratio of LED to  $\alpha$ -source signals for different run periods is presented in Fig. 6. Typical LED amplitudes of calorimeter modules measured during the run are presented in Fig. 7. The gain stability for most of crystals during 35 days of taking data is better than 5%.

#### 2.5. Calibration

Energy calibration of the calorimeter was performed by moving each calorimeter module to the photon beam during special low-intensity calibration runs. The photon flux corresponded to about AAA photons / sec in the energy range  $E_\gamma > 1$  GeV. Energy of each beam photons was determined using GlueX tagging detectors described in Section 1. The typical energy resolution of the beam photon measured with tagger counters is about 0.2%. Flash ADC signal amplitudes in the calorimeter module as a function of the beam energy is presented in Fig. 8. We adjusted PMT high voltages on each module in order to set ADC amplitudes to about 3200 counts for 10 GeV photons and collected data sample for each calorimeter module positioned in the beam. Calibration was subsequently refined by constraining

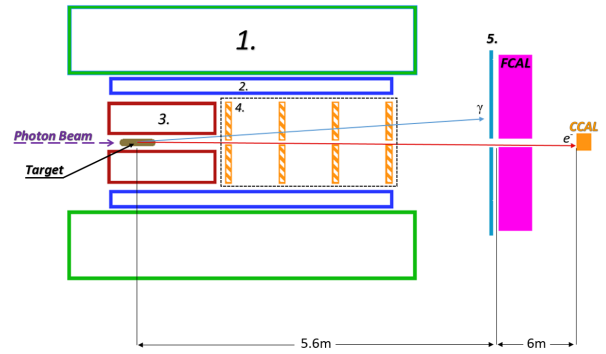


Figure 3: Schematic layout of the GlueX detector.

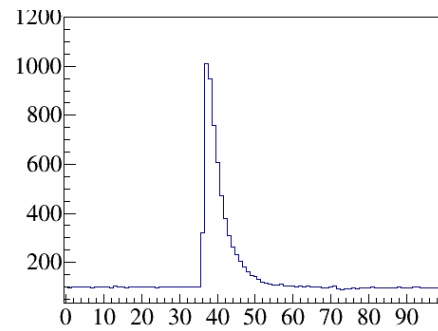


Figure 4: Typical flash ADC signal waveform in the calorimeter module.

the reconstructed energy to the known beam energy determined by the tagger counter. CCAL energy in units of flash ADC counts induced by 10 GeV photons is shown in Fig. 9. The distribution was fit to a Crystal Ball function.

We observed some non-linear performance on the level of a few percents of the active base with the large amplification factor of 24. Some non-linearity effects are presented in Fig. 10 for bases with different amplification factors. After the PrimEx run, we studied the performance of the PMT active bases with different amplification factors. We replaced the original front end electronics in the 3x3 cell calorimeter region with modified bases with the bypassed amplifier. Energy resolution measured in this region is shown in Fig. 10. The energy resolution was fit to the following function. The resolution was found to be about 10% better than that measured with the original base (gain 24). The energy resolution is similar to that of the Hy-Cal calorimeter, which was instrumented with the same type of crystals (produced by SICCAS) and used in several experiments in the Jefferson Lab's experimental Hall B.

#### 2.6. Performance during PrimEx run

Run Conditions for primex - photon flux

CCAL integrated to the global DAQ and trigger - ttrigger types - energy reconstructed in calorimeters, trigger rates - calorimeter rates

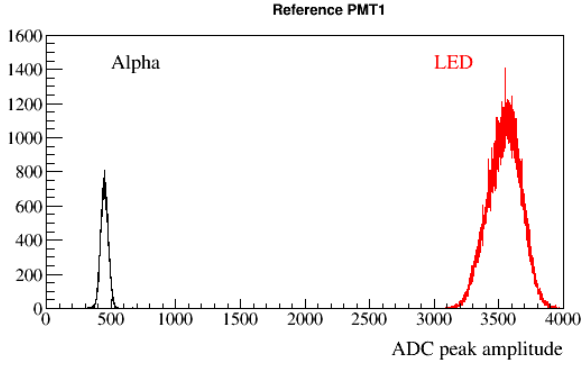


Figure 5: Flash ADC signal amplitudes induced by the LED and  $\alpha$ -source in the reference PMT.

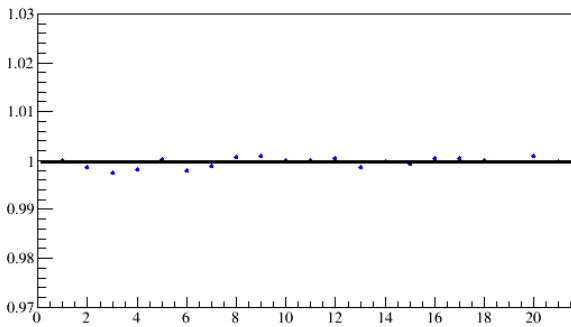


Figure 6: The ratio of LED to  $\alpha$ -source signals for different run periods.

### 2.6.1. Compton reconstruction

## 3. Upgrade of the GlueX forward calorimeter

The forward calorimeter of the GlueX detector is positioned 6 m downstream the beam from the GlueX target, and consists of 2800 lead glass modules, with the size of 4 cm x 4 cm x 40 cm. The typical energy resolution of the FCAL is  $\sigma_{\text{gamma}}/E_{\gamma} = 6.2\%/\sqrt{E} \oplus 4.7\%$ . The calorimeter has been used in several GlueX experiments since 2016. Physics program with the GlueX detector in the experimental Hall D requires an upgrade of the inner part of the forward calorimeter with high-granularity, high-resolution  $\text{PbWO}_4$  crystals. The lead tungstate insert will improve the separation of clusters in the forward direction and the energy resolution of reconstructed photons about a factor of two. We consider to build a 1 m x 1 m insert which will require about 2496 modules. Similar to the CCAL, there will be a 2 module x 2 module beam hole in the middle. The inner layer will be protected by a Tungsten absorber. Crystals are purchased from two vendors: SICCAS (China) and CRYTUR (Czech republic). The size of the FCAL insert may slightly vary depending on availability of funds. Schematic view of the FCAL with the lead tungstate insert is presented in Fig. 13. The  $\text{PbWO}_4$  module design will be essentially the same as for the CCAL, except for some small modifications needed

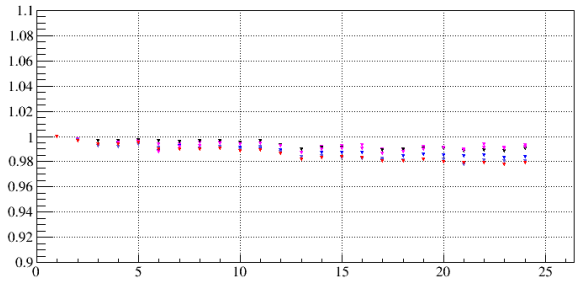


Figure 7: Typical signal amplitudes in calorimeter modules induced by an LED for different PrimEx  $\eta$  run periods. Amplitudes for each module are normalized to the beginning of the run.

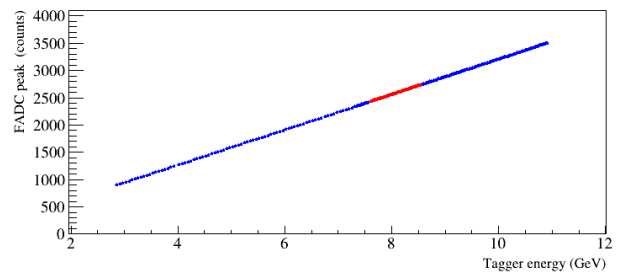


Figure 8: CCAL signal pulse amplitude as a function of the beam energy.

to handle the magnetic field present in the FCAL region.

### 3.0.2. Magnetic field measurement

The longitudinal (directed along the beamline) and transverse (directed perpendicular to the axis of the beamline) components of the magnetic field produced by the GlueX solenoid magnet in the FCAL  $\text{PbWO}_4$  insert area varies between 40 - 50 Gauss and 0 - 8 Gauss, respectively. The longitudinal field is the largest on the beamline, where the transverse component is practically absent. We studied the PMT magnetic shielding using a prototype consisting of an array of 3x3 PMT soft iron (1020 steel) housings, which was positioned in the middle of Helmholtz coils. Each housing had a size of 20.6 mm x 20.6 mm x 100 mm with a 19.9 mm round hole in the middle for the PMT. This corresponds to the realistic size of the magnetic shield, which will be used in the calorimeter module assembly. Inside the housing we inserted two layers of  $\mu$ -metal Co-NETIC cylinders, with the thickness of 350  $\mu\text{m}$  and 50  $\mu\text{m}$ , separated from each other by a Kapton film. The thickest cylinder was spot welded and annealed.

The Helmholtz coils had a diameter of about 1 m and can generate a uniform magnetic field with variable strength below 100 Gauss. A Hole probe was inserted to the central module of the prototype to measure magnetic field at different Z-positions along the PMT side. The field was measured for two different orientations of the prototype with respect to the magnetic field: field oriented along the PMT (longitudinal,  $B_z$ ) and perpendicular to the PMT housing (transverse,  $B_x$ ). Field measurements



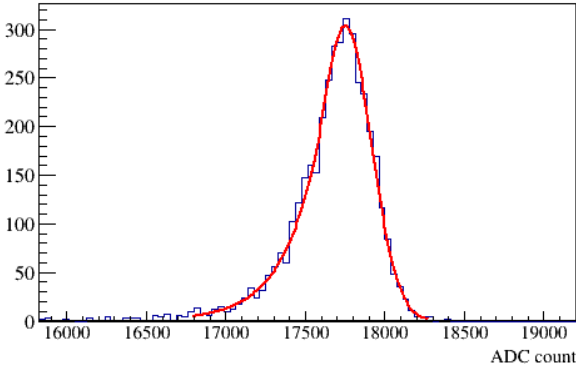


Figure 9: Measured energy in units of flash ADC counts produced by 10 GeV beam photons. The spectrum is fit with a Crystal Ball function.

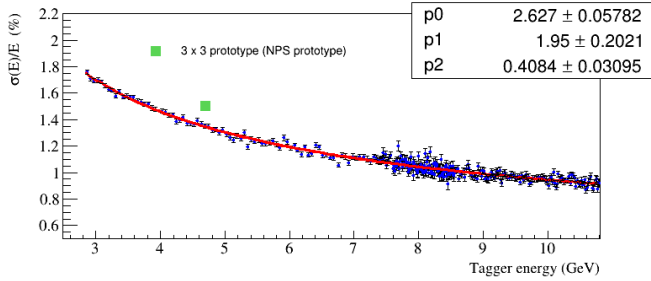


Figure 10: Energy resolution measured in the 3x3 cell region as a function of the photon energy.

are presented in Fig. 14. The PMT shield allowed to significantly reduce both the longitudinal and transverse fields to the level of  $B_z \sim 1$  Gauss and  $B_x \ll 1$  Gauss, respectively. The transverse field, which is well shielded, is more critical for the PMT operation, as it is directed perpendicular to the electron trajectory inside the tube and deflects electrons resulting in the degradation of the photon detector efficiency and gain. The field reaches a plateau at  $Z = 3$  cm from the face of the housing. We will use a 3.5 cm long acrylic light guides, in order to place the PMT area between the photocathode and the last dynode (4.6 cm long) in the region with the smallest magnetic field, as shown in Fig. 14.

We studied performance of the shielded PMT in the magnetic field using an LED pulser. The red LED was placed about 20 cm from the shield and the light diffuser in the middle. The PMT response was measured for different pulse amplitudes and operational HVs. In order to study contributions from longitudinal and transverse field components we rotated the prototype by different angles. Signal amplitudes as a function of the magnetic field are presented on the left plot of Fig. 15. Amplitudes, normalized to measurements without magnetic field are shown on the right plot. The relative degradation of the signal amplitude at  $B = 50$  Gauss ( $B_z = 49$  Gauss and  $B_x = 8.6$  Gauss) was measured to be less than 1%.

### 3.0.3. Light guide studies

Studies of the magnetic shielding demonstrated that the PMT has to be positioned inside the  $\mu$ -metal cylinder about 3 cm from the face of the  $\text{PbWO}_4$  crystal. Light from the crystal will be transmitted to the PMT using a 3.5 cm long acrylic cylindrical lightguide with a diameter of 18.5 cm. The light guide is wrapped with the reflective ESR foil. The light guide will be attached to the PMT with Dymax 3094 UV curing glue. Optical coupling to the crystal will be provided using a 1 mm thick transparent rubber made of the room temperature vulcanized silicon compound, RTV615. This type of material has a widespread application in photodetectors and simplifies the module design. The silicon cookie is not glued to the light guide and the crystal so the module can be easily disassembles if PMT needs to be replaced.

We studied light losses induced by the light guide using a secondary beam of electrons provided by the Hall D pair spectrometer (PS) [1]. The main goal of the PS is to monitor the flux of beam photons delivered to the experimental hall. This is done by reconstructing electromagnetic electron-positron pairs produced by the photons in a thin converter inserted to the beam. Leptons are deflected in a dipole magnet and detected using two scintillator detectors placed in the electron and positron arms of the spectrometer. Each detector consists of 145 tiles, which cover the energy range between 3 GeV and 6 GeV. We positioned several fabricated  $\text{PbWO}_4$  modules behind the PS detector of the electron arm around 4 GeV and compared light yields of two module configurations: (1) the PMT was directly attached to the crystal using an optical grease in the same way as it was done in the CCAL (2) the same PMT and crystal were connected to each other using an optical light guide as described above. Relative light collection of these two configurations were estimated by measuring flash ADC amplitudes induced by PS electrons. Coincidence of hits between the PS tile and lead tungstate module was required. An example of signal pulse amplitudes obtained in the test module as a function of the PS tile are presented in Fig. 1 for the configurations with and without light guide. Light guide results in the typical losses of light of about 15%. We note, that wrapping light guide with the reflective material is important. Losses in unwrapped light guide constitute about 35%.

### 3.0.4. Detector rates

The GlueX detector was designed to carry out experiments using a continuous-energy secondary beam of photon produced by a 12 GeV beam of electrons via bremsstrahlung process. The maximum luminosity corresponds to a photon flux of  $5 \cdot 10^7$   $\gamma$ /sec in the energy range between 8 GeV and 9 GeV incident on a 30 cm long liquid hydrogen target. The designed luminosity was achieved in the Fall run of 2019. This luminosity is about a factor of 2.5 larger than that in the PrimEx experiment, where the CCAL was originally utilized. We performed a study of the CCAL performance in GlueX runs at high luminosity. PMT anode current is one of the critical characteristics, which has to be considered during the design of the PMT divider. Typically the anode current should be on the level of a few micro amperes and significantly smaller than the divider

330 current in order to provide stable performance of the PMT base  
 331 and prevent from long-term degradation of the PMT[. The anode  
 332 current was measured with a special random trigger, which  
 333 was used to read out flash ADC raw data for each CCAL channel  
 334 in a time window of 400 ns. The window size corresponds  
 335 to 100 flash ADC samples. The average ADC voltage in the  
 336 readout window was determined by summing up amplitudes  
 337 and normalizing them to the window size. The voltage measured  
 338 by the ADC is produced by the current going through the  
 339 termination resistor of  $\sim 50 \Omega$ . The anode current can be estimated  
 340 as

$$341 \quad A = \frac{\bar{A}}{R} \cdot \frac{1}{G}, \quad (1)$$

342 where  $A$  is the average ADC amplitude in units of Volts,  $R$  is  
 343 the termination resistor, and  $G$  is the amplifier gain equals to 24.  
 344 The typical anode current measured in CCAL modules in different  
 345 detector layers situated at different distance from the beam  
 346 line is presented in Fig. 16. The rate in the detector is dominated  
 347 by the forward-directed electromagnetic background. The anode  
 348 current is the largest in the innermost layer of the detector  
 349 closest to the beam line and constitutes to about  $1.4 \mu\text{A}$ . This  
 350 current can be compared to the PMT divider current of  $300 \mu\text{A}$ .  
 351 The CCAL measurements can be used to estimate anode current  
 352 in the FCAL lead tungstate insert. The largest PMT current in  
 353 the  $\text{PbWO}_4$  module closest to the beam line is conservatively  
 354 estimated to be about  $20 \mu\text{A}$  if no amplifier is used and the  
 355 PMT base is operated at 1 kV. The detector rate drops rapidly  
 356 with the increase of the radial distance from the beamline. We  
 357 are considering to instrument PMTs in a few inner layers with  
 358 an amplifier with the gain of 5 and do not use the amplifier on  
 359 other modules.

#### 360 4. Neutral Particle Spectrometer

361 The neutral-particle spectrometer (NPS) offers unique scientific  
 362 capabilities to study the transverse spatial and momentum  
 363 structure of the nucleon in the Jefferson Lab experimental Hall  
 364 C. Five experiments have been currently approved using the  
 365 NPS. The experiments and run conditions are listed Table 1. 383

366 The Neutral Particle Spectrometer consists of 1080  $\text{PbWO}_4$  384  
 367 crystals, which will form and an array of 30x36 modules. Crystals  
 368 with the same size as in the CCAL purchased from two 385  
 369 vendors: the CRYTUR and SICCAS. Crystals will be placed 386  
 370 in the frame build from carbon plates and separated from each 387  
 371 other by a 0.5 mm-thick carbon layer to ensure good positioning. 388  
 372 Hamamatsu R4125 PMTs will be attached to the back side of 389  
 373 of each module and be separated from each other with a 0.5 390  
 374 mm thick  $\mu$ -metal plates to reduce the 200 Gauss magnetic field 391  
 375 originating from the sweeping magnet. Blue LED will be used 392  
 376 to calibrate modules and cure crystals degraded due to radiation. 393  
 377 Light from the LED will be distributed through quartz 394  
 378 optical fibers to each individual module. 395

379 The detector is positioned in a temperature controlled frame 396  
 380 on the movable platforms, which will allow to place the detector 395  
 381 at different angles. 396

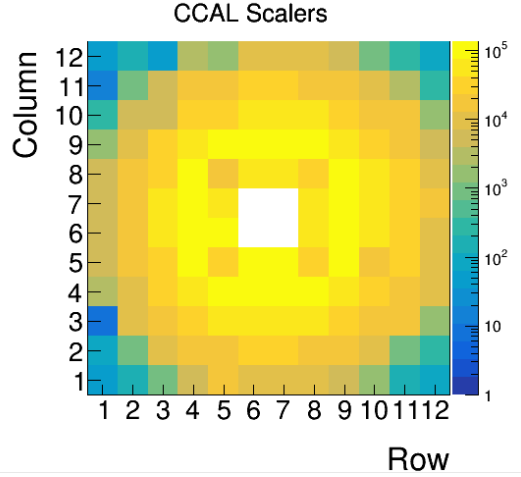


Figure 11: Rates of the CCAL modules during PrimEx  $\eta$  production run. The energy threshold corresponds to 30 MeV.

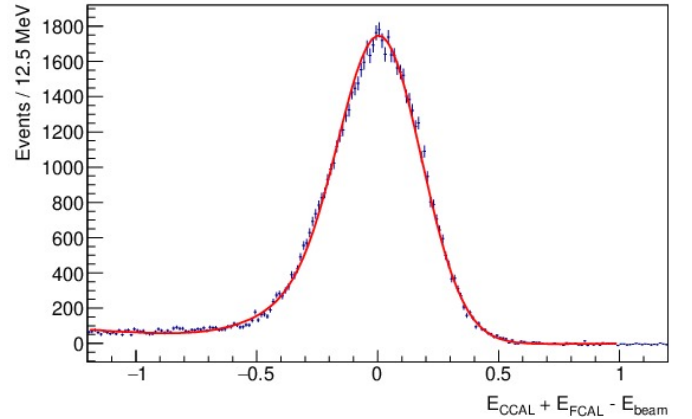


Figure 12: Elasticity distribution of reconstructed Compton candidates.

#### 5. Summary

We have described the design and fabrication details of the pair spectrometer hodoscope, an array of thin scintillator tiles. Light from each tile is detected using a 3 mm x 3 mm Hamamatsu SiPM. A detector prototype was built to perform light collection studies using relativistic electrons produced in the experimental Hall B at Jefferson Lab. Two arms of the hodoscope detector were commissioned and installed in the experimental Hall D.

#### 6. Acknowledgments

This work was supported by the Department of Energy. Jefferson Science Associates, LLC operated Thomas Jefferson National Accelerator Facility for the United States Department of Energy under contract DE-AC05-06OR23177. We would like to thank ...

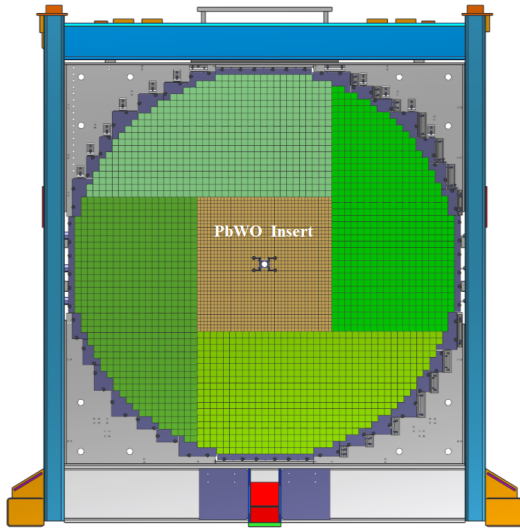


Figure 13: FCAL frame with calorimeter modules installed:  $PbWO_4$  4 crystals (brown area), lead glass blocks (green).

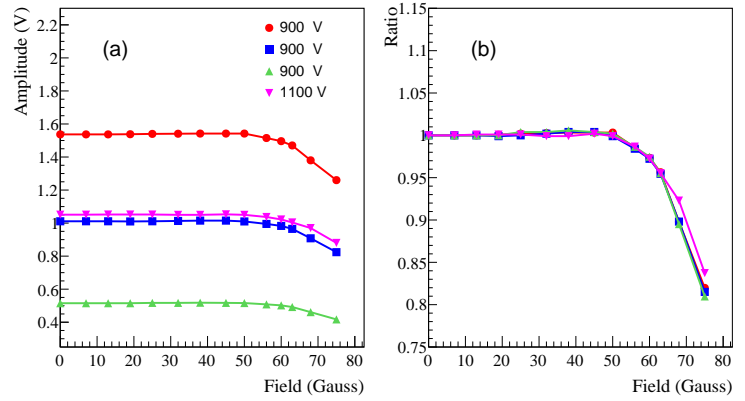


Figure 15: Signal amplitudes of shielded PMT induced by an LED as a function of the magnetic field (a). Amplitudes, normalized to measurements without magnetic field (b). PMT response was measured for different intensities of light pulse and HV settings as shown by different polymarkers.

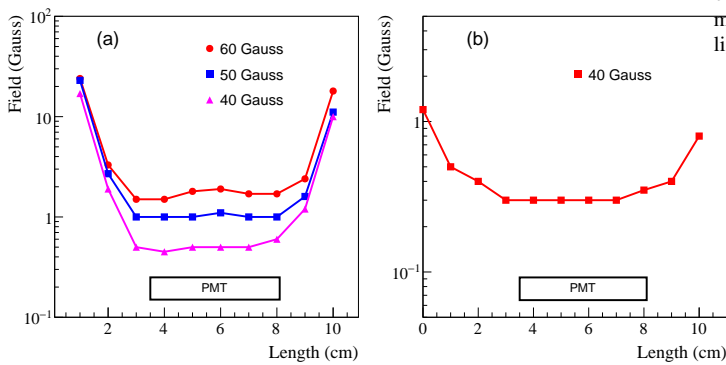


Figure 14: Magnetic field distribution inside the shield housing as a function of the distance from the housing face. Plot (a) corresponds to the longitudinal field and plot (b) corresponds to the transverse field. Markers correspond to different fields produced by Helmholtz coils.

## References

- [1] V. Popov and H. Mkrtychyan *et al.*, Proceedings of the IEEE conference, California, 2012.
- [2] JLab Experiment E12-06-102, (2006) [http://www.jlab.org/exp\\_prog/proposals/06/PR12-06-102.pdf](http://www.jlab.org/exp_prog/proposals/06/PR12-06-102.pdf).
- [3] D. I. Sober *et al.*, Nucl.Inst.and Meth. A, 440 (2000),p.263.
- [4] F. Barbosa *et al.*, Proceedings of IEEE Nuclear Science Symposium, Hawaii, USA (2007).
- [5] F. Barbosa *et al.*, Proceedings of IEEE Nuclear Science Symposium, Virginia, USA (2002).

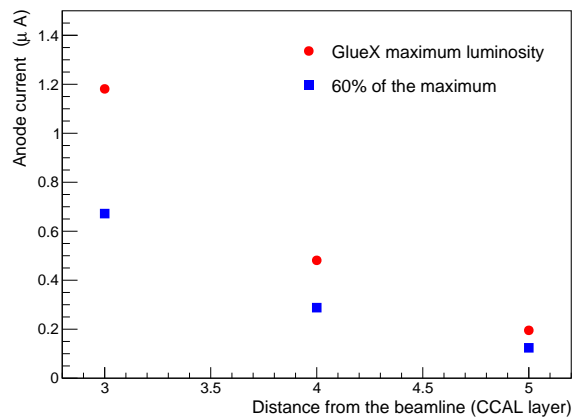


Figure 16: PMT anode current of CCAL modules for different layers.